Stability Analysis and Bifurcations in Soret Convection within a Shallow Porous Enclosure

Conference Paper · January 2004

CITATIONS
0

READS
39

4 authors:

Mahmoud Mamou
National Research Council Canada
257 PUBLICATIONS **2,188** CITATIONS
SEE PROFILE

M. Bourich
Cadi Ayyad University
25 PUBLICATIONS **384** CITATIONS
SEE PROFILE

Mohammed Hasnaoui
Cadi Ayyad University
225 PUBLICATIONS **2,726** CITATIONS
SEE PROFILE

A. Amahmid
Cadi Ayyad University
83 PUBLICATIONS **1,012** CITATIONS
SEE PROFILE

STABILITY ANALYSIS AND BIFURCATIONS IN SORET CONVECTION WITHIN A SHALLOW POROUS ENCLOSURE

M. Bourich[1], M. Hasnaoui[1], M. Mamou[2] and A. Amahmid[1]

[1]*Faculty of Sciences Semlalia, Physics Department, Marrakesh, Morocco*

[2]*Institute for Aerospace Research, National Research Council Canada*
Ottawa, ON, K1A 0R6, Canada

Email: *hasnaoui@ucam.ac.ma*

ABSTRACT

The present study concerns a stability analysis of a Soret convection within a porous layer subject to uniform fluxes of heat and solute on its horizontal boundaries. The solutal buoyancy forces are induced by the imposition of a solute gradient and by the thermal diffusion phenomenon. The Brinkman-extended Darcy model and the Boussinesq approximation are used to model the convective flow through the porous medium. Based on linear stability theory, the resulting linear perturbed equations are solved numerically using the finite element method. An analytical solution is derived on the basis of the parallel flow approximation, and validated against the numerical results obtained by solving the full governing equations using a finite difference method. The results corresponding to the cases of double-diffusive convection (without Soret effect) and Soret convection (with zero mass flux) are recovered by the present formulation as limiting cases. The two other limiting cases, namely the low porosity Darcy porous medium and the clear fluid medium emerge also from the present investigation. The critical Rayleigh numbers for the onset of subcritical and stationary convection are determined explicitly as functions of the governing parameters. The threshold of Hopf bifurcation is determined as function of the governing parameters by performing a linear stability analysis of the perturbed rest state. The existence of two co-dimension-2points (subcodimension-2 and Hopf-codimension-2) is proved and different flow regimes are delineated. The diagrams of stability show that there exists a range of Lewis number in which the subcritical convection disappears. It is shown that the thermal diffusion, has a strong effect on the instability thresholds and on heat and mass transfer characteristics.

1. INTRODUCTION

The Soret phenomenon, which results into separation of components inside a fluid-mixture, has received a growing attention during the last decades. The horizontal systems of a multi-components fluid have received considerable interest due to their practical importance in many engineering applications such as geophysics, geosciences, hydrology and petrology. Compared to the case of pure fluid convection, the Soret effect induces a variety of phenomena exhibiting different convective dynamics and flow structures in binary mixtures. Oscillatory and subcritical flows, hysterisis loops, traveling waves and Hopf bifurcations are some examples of these phenomena. A literature review shows that a great interest is paid to Soret convection in multi-component fluids like the normal ^{3}He-^{4}He, ethanol-water and various gas mixtures. Knobloch and Moore [1] examined the linear stability of experimental Soret convection in a binary fluid mixture for different thermal boundary conditions. The normal ^{3}He-^{4}He and ethanol-water mixtures were considered with no-slip boundary conditions for the velocity and zero outward mass flux for the solute. By using a linear stability analysis, the thresholds for the onset of stationary and oscillatory convection were predicted for different flow mixtures and thermal boundary conditions. The codimension-2 point and the lowest observable frequency along the Hopf bifurcation curve were determined. Batiste et al. [2] considered oscillatory binary fluid convection in a finite container using realistic boundary conditions. They presented results for two systems, ^{3}He-^{4}He and water-ethanol mixtures, for an enclosure aspect ratio

greater than or equal to four. The threshold of oscillatory convective flow and its frequency were predicted using a linear stability analysis. Their results indicated that the enclosure side walls effect is significant even for large aspect ratios and caused the convective flow behavior to be more complex within the enclosure. Competition between odd and even convective modes was observed and examined for different values of the enclosure aspect ratio and the Soret coefficient. Brand et al. [3] developed an amplitude solution for thermal convection in a binary mixture saturated porous media near the codimension-2 point. A constant concentration was assumed on the horizontal boundaries. Results for the threshold of oscillatory and stationary convection were predicted by performing a linear stability analysis. Part of these theoretical predictions, were confirmed by experimental observations in a normal-fluid ^{3}He-^{4}He mixture by Rehberg and Ahlers [4] and Ahlers and Rehberg [5]. Bourich et al. [6] studied analytically and numerically the nonlinear convective flows within a porous layer saturated with a binary mixture. By considering uniform flux boundary conditions with zero mass flux on the horizontal walls, the thresholds of the onset of subcritical and stationary convection were derived for a shallow horizontal layer. Soret-driven thermosolutal convection in a horizontal layer heated and cooled from below and above, respectively, with a constant heat flux was conducted analytically and numerically by Bourich et al. [7]. A comparative study was performed for Darcy porous and clear fluid media. The thresholds for subcritical, oscillatory and stationary convection were obtained explicitly as functions of the governing parameters. The existence of a hysteresis loop when the thermal and solutal buoyancy forces are opposing each other was predicted. Using an appropriate normalization for the Rayleigh number, closing form correlations were derived for the flow intensity and for the heat transfer induced by the interaction between heat flux and Soret diffusion effect.

The present study concerns Soret convection within a porous layer subjected to uniform fluxes of heat and solute on its horizontal boundaries. The main objective of the present study is to investigate the influence of the thermal diffusion on the thresholds of instabilities, flow characteristics and heat and mass transfer, in the presence of imposed mass flux. A dimensionless parameter M, is introduced such as the cases where the double-diffusive convection problems with and without Soret effect can be recovered. In a shallow enclosure, an analytical solution is derived using the parallel flow approximation to predict the critical Rayleigh numbers for the onset of supercritical and subcritical convection. A linear stability analysis is also carried out to predict the onset of over-stabilities. The features predicted by the theoretical analytical analysis are validated against the numerical solutions within a wide range of the governing parameters.

2. MATHEMATICAL MODEL

The system under study is a two-dimensional porous layer of length L' and height H'. The origin of the coordinate system (x' is the horizontal axis and y' is the vertical axis opposing gravity) is at the center of the layer. The vertical end walls of the layer are adiabatic and impermeable while the horizontal walls are subject to uniform fluxes of heat, q', and mass, j'. The porous matrix is assumed isotropic, homogeneous, and the flow obeys to the Brinkman-Hazen-Darcy model using the Boussinesq approximation. Using the vorticity and the stream-function formulation, the dimensionless governing equations are given as follows:

$$\eta\frac{\partial\zeta}{\partial t}+\frac{\mathrm{Da}}{\varepsilon'^{2}\,\mathrm{Pr}}\left(u\frac{\partial\zeta}{\partial x}+v\frac{\partial\zeta}{\partial y}\right)+\zeta=\mathrm{Da}_e\nabla^2\zeta-R_T\left(\frac{\partial T}{\partial x}+N\frac{\partial S}{\partial x}\right) \tag{1}$$

$$\frac{\partial T}{\partial t}+u\frac{\partial T}{\partial x}+v\frac{\partial T}{\partial y}=\nabla^2 T \tag{2}$$

$$\varepsilon\frac{\partial S}{\partial t}+u\frac{\partial S}{\partial x}+v\frac{\partial S}{\partial y}=\frac{1}{\mathrm{Le}}(\nabla^2 S+M\nabla^2 T) \tag{3}$$

$$\nabla^2\psi=-\zeta \tag{4}$$

and the hydrodynamic, thermal and solutal boundary conditions are as follows:

$$x=\pm A_r/2:\ \psi=0,\ \frac{\partial\psi}{\partial x}=0,\ \frac{\partial T}{\partial x}=0,\ \frac{\partial S}{\partial x}=0 \tag{5a}$$

$$y=\pm 1/2:\psi=0,\frac{\partial\psi}{\partial y}=0,\frac{\partial T}{\partial y}=-1,\ \frac{\partial S}{\partial y}=-1+M \tag{5b}$$

In addition to the usual parameters governing the problem, namely, the thermal Darcy-Rayleigh number, $R_T=g\beta_T K\Delta T'H'/(\alpha\nu)$; the Lewis number, $Le=\alpha/D$; the buoyancy ratio, $N=\beta_S\Delta S'/(\beta_T\Delta T')$, the effective Darcy number, $Da_e=\mu_e K/(\mu H'^2)$, and the aspect ratio of the cavity, $A_r=L'/H'$, another dimensionless parameter, M, which characterizes the Soret effect, appears in the governing equations. It is defined as $M=D_T S_0\Delta T'/(D\Delta S')$, where $\Delta T'=q'H'/\lambda$ and $\Delta S'=j'H'/D$. The Nusselt and the Sherwood numbers are defined as follows:

$$\mathrm{Nu}=1/[T(0,-1/2)-T(0,\ 1/2)] \tag{6a}$$

$$\mathrm{Sh}=1/[S(0,-1/2)-S(0,\ 1/2)] \tag{6b}$$

3. NUMERICAL METHOD

The numerical solution of the full governing equations is obtained using a finite-difference method (see, Amahmid et al. [8]), For large aspect ratio enclosures, non-uniform grids were used in the x-direction to capture the flow details near the enclosure end walls and also in the y-direction to obtain a finer grid in the close vicinity of the horizontal walls. The computations reported in this paper were performed with a grid size of 121×61 for A_r=4 and 201×81 for $A_r \geq 8$.

4. ANALYTICAL SOLUTION

The analytical solution is developed for a steady-state flow using a parallel flow assumption (see, Mamou et al. [9]), which leads to the following approximations: $\psi(x, y)= \psi(y)$, $T(x, y) = C_T x + \theta_T(y)$ and $S(x, y) = C_S x + \theta_S(y)$ where C_T and C_S are respectively unknown constant temperature and concentration gradients in the x-direction. Using these approximations together with the boundary conditions (5), Eqs (1)-(3) reduce to a set of ordinary differential equations for which the solution is obtained as:

$$\psi(y) = \psi_0 \frac{H(y)}{H(0)} \tag{7}$$

$$\theta_T(y) = -y + C_T \psi_0 \frac{K(y)}{H(0)} \tag{8}$$

$$\theta_S(y) = (M-1)y + \psi_0 (LeC_S - MC_T) \frac{K(y)}{H(0)} \tag{9}$$

where ψ_0 is the stream function value at the center of the layer, given by:

$$\psi_0 = \frac{H(0)}{2}(C_T + NC_S)R_T \tag{10}$$

with

$$\left.\begin{aligned} H(y) &= \frac{\cosh(\Omega y) - \cosh(\Omega/2)}{\Omega \sinh(\Omega/2)} - y^2 + \frac{1}{4} \\ K(y) &= \frac{\sinh(\Omega y) - \Omega \cosh(\Omega/2) y}{\Omega^2 \sinh(\Omega/2)} - \frac{y^3}{3} + \frac{y}{4} \end{aligned}\right\} \tag{11}$$

and $\Omega=Da_e^{-1/2}$.

Introducing the expressions for C_T and C_S (obtained by performing an energy and mass balance at any cross section of the layer, not given here) into Eq. (10) yields to a fourth-order polynomial in terms of ψ_0 for which the following solutions are:

$$\left.\begin{aligned} \psi_0 &= 0 \\ \psi_0 &= \pm \frac{\left[-b \pm \sqrt{b^2 - 4\,Le^2 c}\right]^{1/2}}{2H(0)\sqrt{2B(Da_e)}Le} \end{aligned}\right\} \tag{12}$$

with $b = 1 + Le^2 - Le(Le + N)R_T^0$ and $c = 1 - \left[1 + NLe - (1 + Le)NM\right]R_T^0$. The parameter R_T^0 represents the normalized Rayleigh number, $R_T^0 = R_T / R^{sup}$, with $R^{sup} = 1/A(Da_e)$. The constants $A(Da_e)$ and $B(Da_e)$ are obtained as follows

$$\left.\begin{aligned} A(Da_e) &= -\frac{2}{f(\Omega)} + \frac{1}{\Omega^2} + \frac{1}{12} \\ B(Da_e) &= \frac{6}{f(\Omega)^2} + \frac{1}{\Omega^2 f(\Omega)} - \frac{1}{3f(\Omega)} \\ &\quad - \frac{1}{8\Omega^2} - \frac{2}{\Omega^4} + \frac{1}{120} \end{aligned}\right\} \tag{13}$$

with $f(\Omega) = 4\Omega \tanh(\Omega/2)$. The expressions of the Nusselt and the Sherwood numbers become

$$\left.\begin{aligned} Nu &= \frac{1 + \Psi_n^2}{1 + \Gamma \Psi_n^2} \\ Sh^{-1} &= \frac{1 - M}{Sh(M=0)} + \frac{4M(1 + Le)\Psi_m^2}{[1 + \Psi_n^2][1 + Le^2 \Psi_n^2]} \end{aligned}\right\} \tag{14}$$

with $Sh(M=0) = \dfrac{1 + \Psi_n^2}{1 + \Gamma Le^2 \Psi_n^2}$, $\Gamma = (B - A^2)/B$, $\Psi_n^2 = 4H(0)^2 A(Da_e)^2 \psi_0^2$ and $\Psi_m^2 = \psi_n^2 A^2 / B$.

According to Eq. (12), the parallel flow solutions exist only when the conditions $-b \pm \sqrt{b^2 - 4\,Le^2 c} > 0$ and $b^2 - 4\,Le^2 c > 0$ are satisfied. According to these conditions, the (N, Le) plane can be divided into different regions and their extents depend on weather M≤0 or 0≤M<1, or M≥1. In the first region, the parallel flow does not exist. In the second and third regions the only possibility is the existence of supercritical convection. However, in the fourth and fifth regions both subcritical and supercritical convection are possible. The supercritical Rayleigh number, characterizing the transition from the rest state to stationary convective regime, through zero flow amplitude, is given by

$$R_{TC}^{sup} = \frac{R^{sup}}{[1 + NLe - (1 + Le)NM]} \tag{15}$$

The threshold R_{TC}^{sub}, marking the onset of subcritical convection, characterized by a transition from the quiescent state to finite amplitude convection, is given by

$$R_{TC}^{sub} = \frac{R^{sup}(1+Le)}{Le(Le+N)^2}\left[\sqrt{Le(Le+NM-1)} + \sqrt{N(1+Le(M-1))}\right]^2 \quad (16)$$

Two limiting cases can be recovered. The first one corresponds to a double diffusive convection (Amahmid et al. [9]) in which the Soret effect was neglected (M=0). The second case concerns the Soret effect [7] for which a zero mass flux (j'=0) was imposed on the horizontal boundaries. For the latter case, the results are deduced from the present study by making $N\to 0$, $M\to\infty$ and $MN\to -\varphi$.
Also, the results corresponding to Darcy porous and pure fluid media can be deduced from the Brinkman-Hazen-Darcy model.

4.1 Case of Darcy Porous Medium (Da_e<<1)

For Da_e<<1, the expressions of ψ, T, S, ψ_0, Nu and Sh reduce to :

$$\psi(y) = \psi_0(1-4y^2) \quad (17)$$

$$T(x,y) = C_T x - y - C_T\psi_0\left(\frac{4}{3}y^3 - y\right) \quad (18)$$

$$S(x,y) = C_S x + (M-1)y - \psi_0(LeC_S - MC_T)\left(\frac{4}{3}y^3 - y\right) \quad (19)$$

$$\psi_0 = \pm\frac{1}{8\sqrt{2}Le}\left[-b \pm \sqrt{b^2 - 4Le^2 c}\right]^{\frac{1}{2}} \quad (20)$$

with $b = 120(1+Le^2) - 10Le(Le+N)R_T$ and $c = 14400 - 1200\left[1 + NLe - (1+Le)NM\right]R_T$.

$$\left.\begin{aligned} Nu &= \frac{3(15+8\psi_0^2)}{45+4\psi_0^2} \\ Sh^{-1} &= (1-M)\frac{45+4Le^2\psi_0^2}{3(15+8Le^2\psi_0^2)} + \frac{800MLe\psi_0^2}{(15+8\psi_0^2)(15+8Le^2\psi_0^2)} \end{aligned}\right\} \quad (21)$$

For this limit, the thresholds of convection are obtained from Eqs. (15)-(16) with R^{sup}=12.

4.2 Case of Pure Fluid Medium(Da_e>>1)

For this limit, the expressions of ψ, T, S, ψ_0, Nu and Sh reduce to :

$$\psi(y) = \psi_0(4y^2-1)^2 \quad (22)$$

$$T(x,y) = C_T x - y - C_T\psi_0\left(\frac{16}{5}y^5 - \frac{8}{3}y^3 + y\right) \quad (23)$$

$$S(x,y) = C_S x + (M-1)y - \psi_0(LeC_S - MC_T)\left(\frac{16}{5}y^5 - \frac{8}{3}y^3 + y\right) \quad (24)$$

$$\left.\begin{aligned} Nu &= 10\frac{1+\psi_r^2/70}{10+3\psi_r^2/70} \\ Sh^{-1} &= \frac{1-M}{Sh(M=0)} + \frac{M(1+Le)\psi_r^2/100}{(1+\psi_r^2/70)(1+Le^2\psi_r^2/70)} \end{aligned}\right\} \quad (25)$$

with $Sh(M=0) = \frac{1+\psi_r^2/70}{1+0.3\psi_r^2/70}$ and $\psi_r = \frac{16\psi_0}{3}$.

For this case, the thresholds of convection are deduced from those of Eqs. (15)-(16) with R^{sup}=720.

5. Linear Stability Analysis

To study the stability of the motionless diffusive state and the fully convective developed flows, the stream function, temperature and concentration fields are decomposed as follows:

$$\left.\begin{aligned} \psi &= 0 + e^{pt}\Psi \\ T &= -y + e^{pt}\theta \\ S &= (M-1)y + e^{pt}\phi \end{aligned}\right\} \quad (26)$$

The function Ψ, θ et ϕ are the perturbation profiles, and p is the growth rate of the perturbation. The boundary conditions for the perturbation, according to Eq. (5), are:

$$\Psi = \frac{\partial\Psi}{\partial y} = \frac{\partial\theta}{\partial y} = \frac{\partial\phi}{\partial y} = 0 \quad (27)$$

Substituting Eq. (26) into the governing equations (1)-(3) and neglecting the second-order terms, the linear problem is

$$\left.\begin{aligned}(\eta p+1)\nabla^2\Psi &= Da_e\nabla^4\Psi - R_T\left(\frac{\partial\theta}{\partial x}+N\frac{\partial\phi}{\partial x}\right)\\ p\theta+\frac{\partial\Psi}{\partial x} &= \nabla^2\theta\\ \varepsilon\,Le\,p\phi+Le\frac{\partial\Psi}{\partial x} &= \nabla^2\phi+M\nabla^2\theta\end{aligned}\right\}\quad(28)$$

The linear problem (28) subject to the boundary conditions (27) is solved numerically using the finite element method. The resulting integral form of the equations are obtained as follows:

$$\begin{bmatrix}[K]_\Psi & R_T[B]_{\Psi\theta} & R_T N[B]_{\Psi\theta}\\ [B]_\Psi & [K]_\theta & 0\\ Le[B]_\Psi & M[K]_\theta & [K]_\phi\end{bmatrix}\begin{Bmatrix}\Psi\\ \theta\\ \phi\end{Bmatrix} = p\begin{bmatrix}-\eta[L]_\Psi & 0 & 0\\ 0 & -[L]_\theta & 0\\ 0 & 0 & -\varepsilon Le[L]_\phi\end{bmatrix}\begin{Bmatrix}\Psi\\ \theta\\ \phi\end{Bmatrix}\quad(29)$$

where $[B]_\Psi$, $[B]_{\Psi\theta}$, $[B]_{\Psi\phi}$, $[K]_\Psi$, $[K]_\theta$, $[K]_\phi$, $[L]_\Psi$, $[L]_\theta$ and $[L]_\phi$ are square matrices and their definitions are given by:

$$\left.\begin{aligned}[K]_\Psi &= Da_e\int_\Omega\nabla^2H_j\nabla^2H_i d\Omega\\ &\quad+\int_\Omega\nabla H_j.\nabla H_i d\Omega\\ [L]_\Psi &= [K]_\theta=[K]_\phi=\int_\Omega\nabla H_j.\nabla H_i d\Omega\\ [L]_\theta &= [L]_\phi=\int_\Omega H_jH_i d\Omega\\ [B]_\Psi &= [B]_{\Psi\theta}=[B]_{\Psi\phi}=\int_\Omega\frac{\partial H_j}{\partial x}H_i d\Omega\end{aligned}\right\}\quad(30)$$

with H_i representing the Hermite cubic function and Ω is the domain of computation.

5.1 Onset of Stationary Convection

For stationary convection, p=0, after introducing the boundary conditions, the equations in (29), could be combined to yield the following eigenvalue problem:

$$\left[[E]-\lambda[I]\right]\{\Psi\}=0$$

with $\lambda=\dfrac{1}{R_T[1+NLe-(1+Le)NM]}$.

The threshold for stationary convection is then given by:

$$R_{TC}^{sup}=\frac{R^{sup}}{1+NLe-(1+Le)NM}\quad(31)$$

where $R^{sup}=1/\lambda_{max}$ and λ_{max} represents the maximum eigenvalue.

5.2 Onset of Oscillatory Convection

For a given aspect ratio or wavelength, the onset of the oscillatory convection is obtained by examining the maximum eigenvalue when its value swishes from negative to positive values. When $p_r<0$, the perturbation is decaying, and $p_r>0$ the perturbation is growing. For a sallow porous cavity, the thresholds of the onset of oscillatory convection is given by:

$$R_{TC}^{Hopf}=\frac{(\varepsilon Le+1)}{\varepsilon Le+(1-M)NLe}R^{sup}\quad(32)$$

The above expression shows clearly that the threshold of the oscillatory convection depends not only on N, Le and M, but also on ε. It is therefore obvious that, when N(M-1)>ε, overstabilities do not exist. Note that, in the case corresponding to zero mass flux, the expression for the threshold of oscillatory convection is deduced from Eq. (32) by making M=0.

6. Results and Discussion

6.1 Stability Diagrams

The behavior of the flow and the nature of bifurcations are analyzed via a stability diagrams (Figs. 1(a)-(c)) obtained for M=0.5, ε=0.5 and typical values of Le: (a) Le=0.9, (b) Le=1.9 et (c) Le=10. The stability diagrams are illustrated in the (R_T^0, N) plane. The Rayleigh number is scaled by the parameter R^{sup} ($R_T^0=R_{TC}/R^{sup}$) such that the diagrams remain valid for any effective Darcy number. For a given set of M and N, the number and the nature of the regions delineated in the (N, Le) plane depend on the Le range. In fact, by increasing N, one passes from stationary convection regime to subcritical flow for Le < Le*, and from the stable towards a stationary regimes for Le* < Le < 1/(1-M), or from the stable towards a subcritical convection and then towards the supercritical regimes for Le > 1/(1-M). The expression of Le*, is given by:

$$Le^{*} = \frac{M}{3(1-M)} + \sqrt[3]{-\frac{q}{2} + \sqrt{\left(\frac{p}{3}\right)^{3} + \left(\frac{q}{2}\right)^{2}}} + \sqrt[3]{-\frac{q}{2} - \sqrt{\left(\frac{p}{3}\right)^{3} + \left(\frac{q}{2}\right)^{2}}} \quad (33)$$

with

$$p = \frac{M(2M-3)}{3(M-1)^{2}} \text{ and } q = \frac{20M^{3} - 45M^{2} + 27M}{27(M-1)^{3}}$$

.

This justifies the choice of the different values of Le. The different convective regimes are delineated by the thresholds of stationary (Eq. 15), subcritical (Eq. 16) and Hopf (Eq. 32) convection. In the figures 1(a)-(c), there are four regions in which different flow behaviors may occur. In region (I), the fluid is unconditionally stable, i.e., all dynamic perturbations imposed to the system, regardless of their amplitude, decay with time and the fluid returns always to the rest state. The second region (region II) delineates possible subcritical convection, in which the rest state instability can be triggered only by large finite amplitude perturbations. The oscillatory regime is represented by region (III), in which the rest state of the fluid is unsteady in presence of any perturbations. In this region, the amplitude of perturbation grows in time in an oscillatory manner. The last region (region IV) corresponds to subcritical convection in which the motionless state is unconditionally unstable. Note that, for Le=1.9 the subcritical convection does not exist.

For negative values of M, the obtaining stability diagrams (results not presented) are similar to those presented in Figs. 1(b)-(c), whereas the stability diagram type of Fig 1(a) is not observed. However, for M≥1 only the stability diagram similar to that of Fig. 1(c) is possible.

In the (R_T^0, N) plane, the intersection between the thresholds of subcritical and stationary convection leads to a sub-codimension-2 point which is represented in Figs. 1(a) and 1(c) by a square symbol and its coordinates are given by:

$$\left.\begin{aligned} N^{sub-c2} &= \frac{1}{(M-1)Le^{3} + MLe^{2} + MLe + M} \\ R_T^{0,sub-c2} &= \frac{(M-1)Le^{3} + MLe^{2} + MLe + M}{(M-1)Le^{3} + MLe^{2} + Le} \end{aligned}\right\} \quad (34)$$

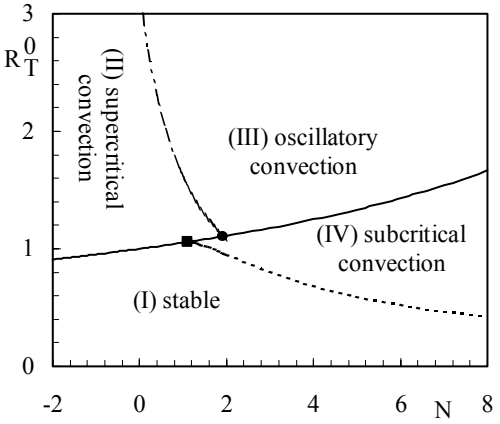

FIG. 1(a): Stability diagram of R_T^0 versus N for M=0.5, Le=0.9, and ε=1.

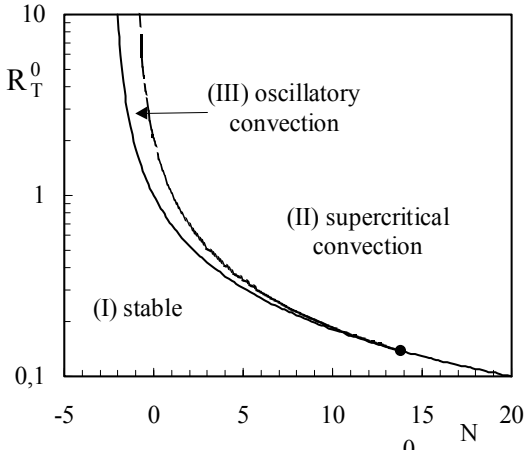

FIG. 1(b): Stability diagram of R_T^0 versus N for M=0.5, Le=1.9, and ε=1.

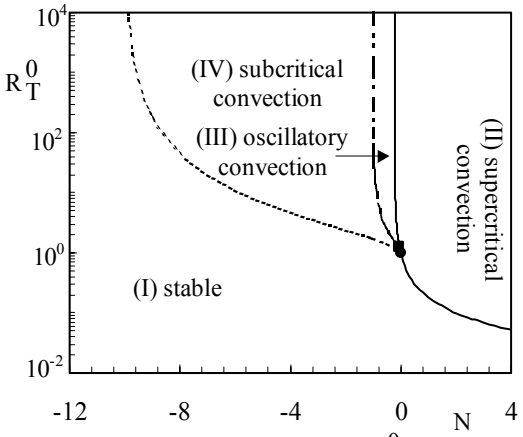

FIG. 1(c): Stability diagram of R_T^0 versus N for M=0.5, Le=10, and ε=1.

The existence of the sub-codimension-2 point depends M when the following conditions are satisfied:

$$\left.\begin{array}{ll} \mathrm{Le} > \dfrac{1}{1-\mathrm{M}} & \text{for } \mathrm{M} < 0 \\ \mathrm{Le} < \mathrm{Le}^{*} \text{ or } \mathrm{Le} > \dfrac{1}{1-\mathrm{M}} & \text{for } 0 \le \mathrm{M} < 1 \\ \forall\, \mathrm{Le} & \text{for } \mathrm{M} \ge 1 \end{array}\right\} \quad (35)$$

For the considered value (M=0.5) in Figs. 1(a)-(c), the sub-codimension-2 point exist for Le<Le*=1.878 or Le>2.

The intersection of the thresholds of stationary and Hopf bifurcations gives a Hopf-codimension-2 point which is indicated on the stability diagram by a circular symbol, Figs. 1(a)-(c), and its coordinates are given by:

$$\mathrm{N}^{\mathrm{Hopf-c2}} = \frac{1}{(\mathrm{M}-1)\varepsilon\mathrm{Le}^2 + \mathrm{M}\varepsilon\mathrm{Le} + \mathrm{M}}$$

$$\mathrm{R}_{\mathrm{T}}^{0,\mathrm{Hopf-c2}} = \frac{(\mathrm{M}-1)\varepsilon\mathrm{Le}^2 + \mathrm{M}\varepsilon\mathrm{Le} + \mathrm{M}}{(\mathrm{M}-1)\varepsilon\mathrm{Le}^2 + (\mathrm{M}(\varepsilon-1)+1)\mathrm{Le}}$$

These coordinates exist only when the following conditions are satisfied:

$$\left.\begin{array}{l} \mathrm{M} > \dfrac{\varepsilon\mathrm{Le}^2}{1+\varepsilon\mathrm{Le}+\varepsilon\mathrm{Le}^2} \\ \mathrm{M} < \dfrac{\varepsilon\mathrm{Le}-1}{\varepsilon\mathrm{Le}+\varepsilon-1} \end{array}\right\} \quad \text{for } \mathrm{Le} > \frac{1-\varepsilon}{\varepsilon}$$

$$\left.\frac{\varepsilon\mathrm{Le}^2}{1+\varepsilon\mathrm{Le}+\varepsilon\mathrm{Le}^2} < \mathrm{M} < \frac{\varepsilon\mathrm{Le}-1}{\varepsilon\mathrm{Le}+\varepsilon-1} \quad \text{for } \mathrm{Le} < \frac{1-\varepsilon}{\varepsilon}\right\}$$

6.2 Effect of M

The parameter M represents the relative strength of the Soret effect with respect to the solutal diffusion. It can be widely varied by considering different working fluids, changing the mean solute concentration or heat and mass flux intensity. Figs. 2(a)-(b) illustrate the effect of M on ψ_0 and Nu for R_T=100, Le=10, Da_e=0.01, and (a) N=-2 and (b) N=3. It should be mentioned that, the thermal diffusion induces an inversion of the concentration gradient sign in the horizontal direction when M exceeds some critical value. Figs. 3(a)-(c) illustrate this behavior in terms of streamlines, isotherms and iso-solutes for R_T=100, Le=3, N=-0.5, Da_e=0.01 A_r=8 and (a) M=2.5, (b) M=3.249, and (c) M=4. The direction of the solute migration depends on whether M is higher or lower than 3.249; it is counterclockwise for M=2.5 and clockwise for M=4, see Fig. 3(a) and (c), respectively. In addition, for $M=M_i$=3.249, the horizontal concentration gradient becomes zero and the mass transfer in the vertical direction is only due to thermal effect and the solutal diffusion is characterized by horizontal iso-solutes (C_S=0). The expression of the critical value M_i, at which the concentration gradient becomes zero in the horizontal direction, is given by:

$$\begin{cases} \mathrm{M_i} = \dfrac{\mathrm{Le}\,\mathrm{R}_{\mathrm{T}}^{0}}{(1+\mathrm{Le})} & \text{for } \mathrm{R}_{\mathrm{T}}^{0} > \dfrac{\mathrm{L}^2-1}{\mathrm{L}^2} \\ \mathrm{M_i} = \dfrac{\mathrm{Le}-1}{\mathrm{Le}} & \text{for } \mathrm{R}_{\mathrm{T}}^{0} < \dfrac{\mathrm{L}^2-1}{\mathrm{L}^2} \end{cases} \quad (38)$$

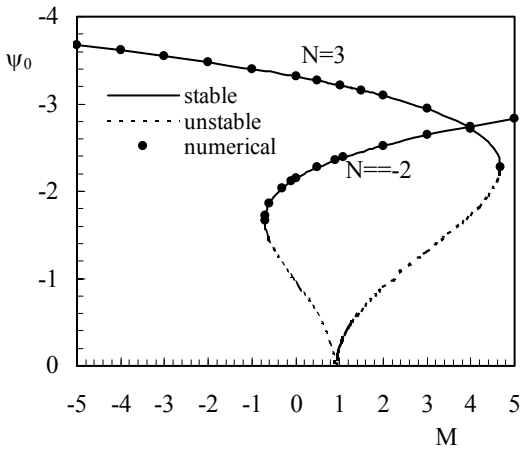

FIG. 2(a): Effect of M on ψ_0 for R_T=100, Le=10 and Da_e=0.01.

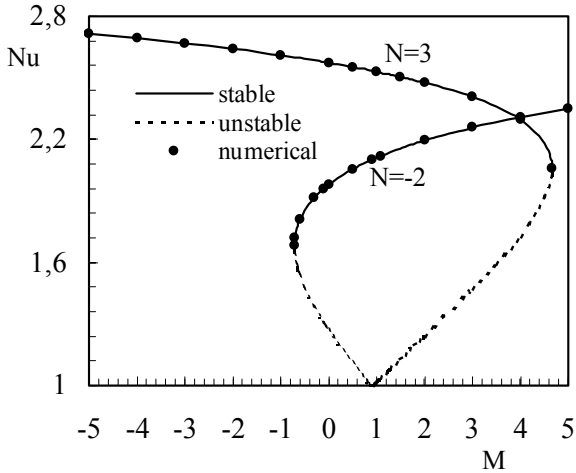

FIG. 2(b): Effect of M on Nu for R_T=100, Le=10 and Da_e=0.01.

Note that, the above-mentioned behaviors have not been observed in the absence of the Soret effect, see Amahmid *et al.* [4].

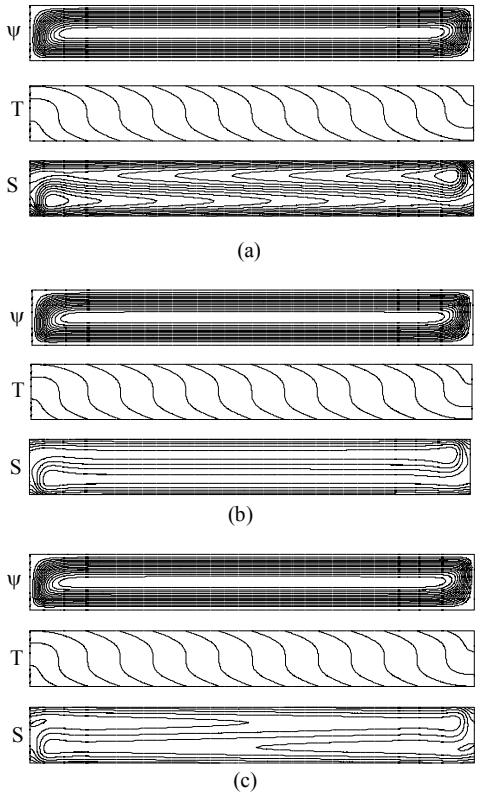

FIG. 3(a)-(c): Streamlines, isotherms and iso-solutes for R_T=100, Le=3, N=-0.5, Da_e=0.01, A_r=8 and (a) M=2.5, (b) M=3.249, and (c) M=4.

7. CONCLUSION

The present analytical and numerical investigation concerns the Soret effect on double-diffusive convection in a horizontal porous layer subjected to uniform fluxes of heat and solute. The mathematical formulation covers the cases of double-diffusive convection without Soret effect and with Soret effect in the case of zero mass flux. In the limit of a shallow enclosure, an analytical closed form solution is derived on the basis of the parallel flow approximation. The thresholds for the onset of stationary and finite amplitude flows are determined explicitly as functions of the governing parameters. The linear stability analysis is used to determine the threshold of Hopf bifurcation. The existence of codimension-2 point is proved and different flow regimes are delineated. It was found that there exists a critical value of M, for which the Soret effect imposes a vertical stratification of concentration. The main features predicted by the analytical solution are confirmed numerically by solving the full governing equations.

REFERENCES

[1]. E. Knobloch and D. R. Moore, Linear stability of experimental Soret Convection, Physical Review A 37, pp. 860-870, 1988.

[2]. O. Batiste, I. Mercader, M. Net and E. Knobloch, Onset of oscillatory fluid convection in finite containers, Physical Review, vol. 59, pp. 6730-6741, 1999.

[3]. H. Brand, P.C. Hohenberg and V. Steinberg, Amplitude equation near a polycritical point for the convective instability of a binary fluid mixture in a porous medium, Physical Review, vol. 27, pp. 591-593, 1983.

[4]. I. Rehberg and G. Ahlers, Experimental observation of a codimension-two bifurcation in a binary fluid mixture, Physical Review Letters, vol. 55, pp. 500-503, 1985.

[5]. G. Ahlers and I. Rehberg, Convection in a binary mixture heated from below, Physical Review Letters, vol. 56, pp. 1373-1376, 1986.

[6]. M. Bourich, M. Hasnaoui, A. Amahmid and M. Mamou, Soret driven thermosolutal convection in a shallow porous enclosure, Int. Comm. Heat Mass Transfer, vol. 29, pp. 717-728, 2002.

[7]. M. Bourich, M. Hasnaoui, M. Mamou and A. Amahmid, Soret effect inducing subcritical and Hopf bifurcations in a shallow enclosure filled with a clear binary fluid or a saturated porous medium: A comparative study, Physics of Fluids, vol. 16, pp. 551-568, 2004.

[8]. A. Amahmid, M. Hasnaoui, M. Mamou and P. Vasseur, Double-diffusive parallel flow induced in a horizontal Brinkman porous layer subjected to constant heat and mass fluxes: analytical and numerical studies, J. Heat Mass Transfer, vol. 35, pp. 409-421, 1999.

[9]. M. Mamou, P. Vasseur and M. Hasnaoui, On numerical stability analysis of double-diffusive convection in confined enclosures, J. Fluid Mech., vol. 433, pp. 209-250, 2001.